Space Charge Behavior in SF_6 Gas and Sequential Generation of PD Pulses

Toshihiro Takahashi, Tatsuji Yamada, Naoki Hayakawa
and Hitoshi Okubo

Department of Electrical Engineering
Nagoya University, Japan

ABSTRACT

We observed time-resolved partial discharge (PD) characteristics under ac and dc conditions in order to demonstrate the effects of space charge behavior and the corona stabilization effect in SF_6 gas. From the experimental results, we found that the charge magnitude of the first PD in the positive half cycle of applied ac voltage depended only on the instantaneous voltage. Under dc conditions we found that the magnitude of the PD charge related closely to the time interval between PD pulses. Space charge behavior and the PD generation mechanism are interpreted diagrammatically, and we describe how positive ions reduce the magnitude of PD charge and activate the corona stabilization effect, and that the negative ions shorten the time interval between PD pulses.

1 INTRODUCTION

SF_6 gas insulated power apparatus like gas-insulated system (GIS) and switchgear have been used widely in electric power transmission and distribution systems [1–3]. However, the insulation performance of SF_6 gas decreases under inhomogeneous electric fields, which is caused by *e.g.* metallic particle contamination [3]. In such cases, PD occurs where the electric field is concentrated and finally PD would lead to breakdown (BD) [4]. Although many PD detection methods have been developed [2, 5–7], most methods have not taken into account the PD generation and suppression mechanism, especially under ac condition. This is because the space charge behavior is very much complicated under ac condition and the PD characteristics are strongly influenced by the space charges. From these viewpoints, detailed investigation of PD mechanisms under ac condition is strongly needed for the insulation diagnosis and reliable prediction of the lifetime of GIS [3].

In this paper, we measured the time-resolved PD characteristics under ac and dc conditions, especially on the space charge behavior in SF_6 gas. Comparison of PD characteristics under ac and dc conditions enabled us to discuss the PD generation mechanism and corona stabilization effect in SF_6 gas.

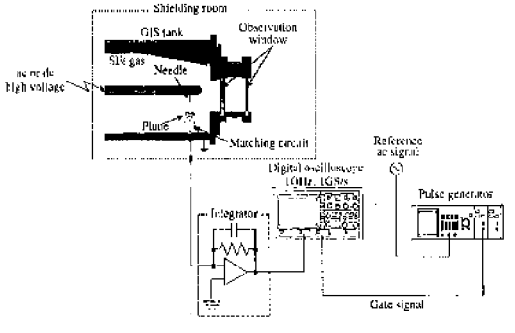

Figure 1. Experimental setup.

2 EXPERIMENTAL

Figure 1 shows the experimental setup. As a PD source, we set a needle electrode (tip radius $r = 500\ \mu$m, length $l = 20$ mm) made of

1070-9878/0/ $3.00 © 2000 IEEE

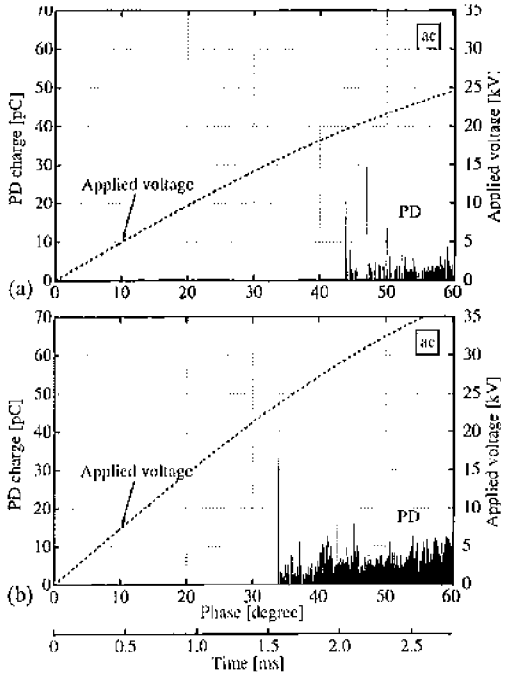

Figure 2. Typical time-resolved PD characteristics at positive PD inception phase for a single power frequency cycle. ($r = 500$ μm, $g = 10$ mm, in SF_6 gas, $P = 0.1$ MPa) (a) $V_a = 20$ kVrms (b) $V_a = 30$ kVrms.

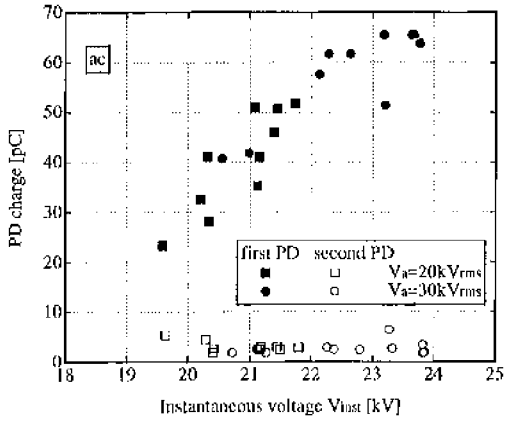

Figure 3. Relationship between PD charge and instantaneous voltage for first and second PD in the positive half cycle.

stainless steel on the HV conductor of a model GIS. We applied ac and dc HV to the model GIS in order to generate PD at the needle tip. A plane electrode was set at 10 mm (gap length $g = 10$ mm) below the needle tip to make an inhomogeneous electric field configuration. PD signals were detected by a digital oscilloscope (sampling rate 1 GS/s, analog bandwidth 1 GHz) through a matching circuit (available for dc ~1 GHz or higher) and an integrator using a high-speed operational amplifier [8] with the charge coefficient of 274 pC/V and the time constant of 33 ns, which determined the sensitivity and the time resolution in our PD measuring system. By selecting the appropriate time and voltage ranges of the oscilloscope, we achieved the time-resolved observation of

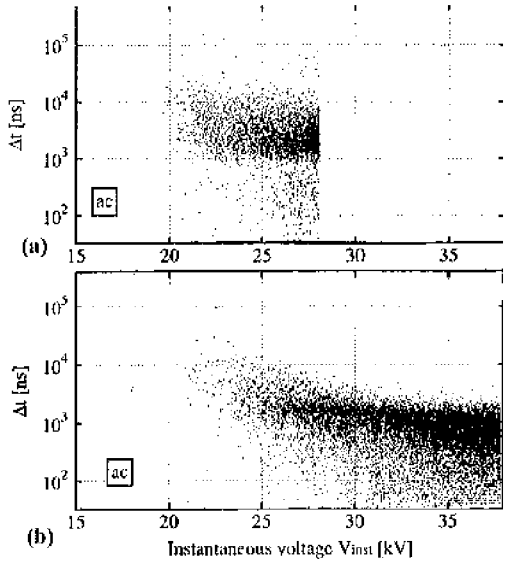

Figure 4. Relationship between time interval Δt between sequential PD pulses and instantaneous voltage. (a) $V_a = 20$ kVrms, (b) $V_a = 30$ kVrms.

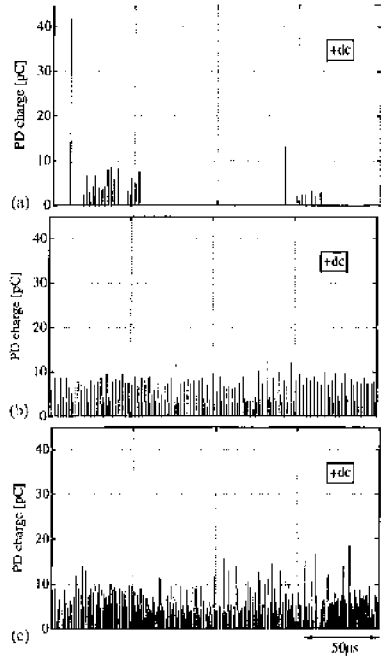

Figure 5. Typical time-resolved PD characteristics under +dc condition. ($r = 500$ μm, $g = 10$ mm, in SF_6 gas, $P = 0.1$ MPa). (a) $V_a = 25$ kV, (b) $V_a = 30$ kV, (c) $V_a = 40$ kV.

individual PD signals. In the case of ac, a signal synchronized with the applied ac voltage was used to trigger the oscilloscope at a designated phase position [9]. The model GIS was filled with SF_6 gas at the pressure $P = 0.1$ MPa and all of the experiments were carried out at room temperature.

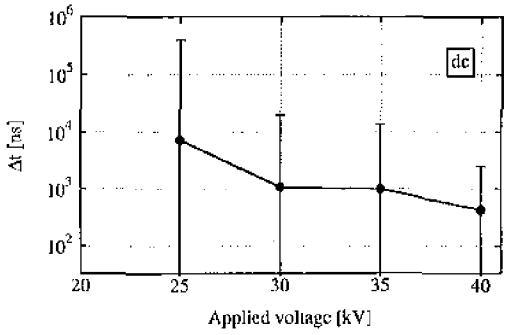

Figure 6. Variation of the time interval Δt between sequential PD pulses with applied voltage.

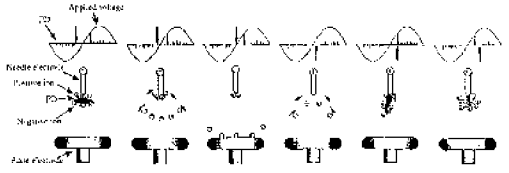

Figure 7. Schematic illustration of the generation mechanism of the first and the subsequent PD in positive half cycle under ac.

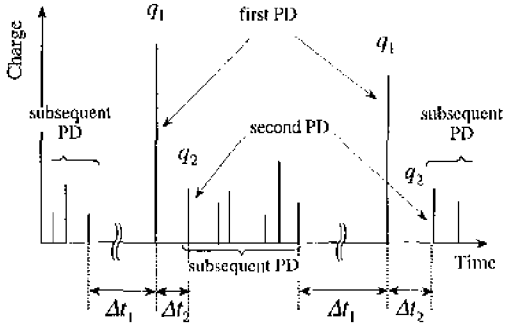

Figure 8. Definition of q_1, q_2, Δt_1 and Δt_2 for sequential PD pulses under dc conditions.

3 EXPERIMENTAL RESULTS

3.1 ac CONDITION

Figure 2 shows the typical time-resolved PD characteristics under ac conditions at (a) applied voltage $V_a = 20$ kVrms and (b) $V_a = 30$ kVrms for a single power frequency cycle. In the Figures, the solid vertical lines show the individual PD pulse and the broken line shows the applied voltage. As seen in Figure 2(a), the first PD with relatively large charge occurred at 44° and was followed by many subsequent PD with small charge magnitudes at $V_a = 20$ kVrms. The sequential generation of the first PD and the subsequent PD was repeated in the identical half cycle. On the other hand, at $V_a = 30$ kVrms in Figure 2(b), the first PD had a larger charge than at $V_a = 20$ kVrms and the subsequent PD with a higher repetition rate were observed in the positive half cycle.

The experiments under the same conditions were carried out 10 times. The resultant relationship between PD charge and the instantaneous voltage for the first PD and the subsequent PD in the positive half cycle is shown in Figure 3. As can be seen in Figure 3, though

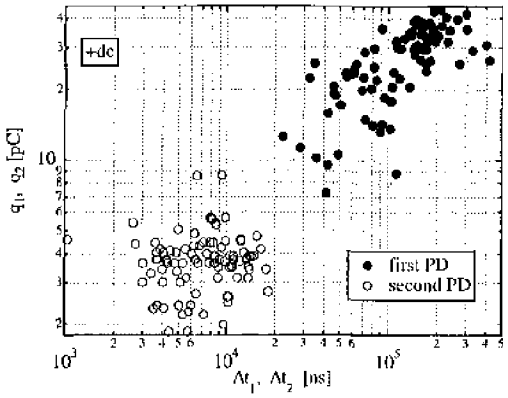

Figure 9. Relationship between sets of q_1 *vs.* Δt_1 and q_2 *vs.* Δt_2 under dc conditions at $V_a = 25$ kV.

the instantaneous applied voltage V_{inst} scattered from 19.5 to 24 kV, the charge magnitude of the first PD was proportional to V_{inst} at the PD generation, independent of the applied voltage V_a. In contrast, the charge magnitude of the subsequent PD was small and independent of V_{inst} and V_a.

Figure 4 shows the relationship between the time interval Δt between sequential PD pulses and V_{inst} at (a) $V_a = 20$ kVrms and (b) $V_a = 30$ kVrms, respectively. Note that V_{inst} in Figure 4 shows the instantaneous voltage at the second PD of the two sequential PD pulses. At $V_a = 20$ kVrms in Figure 4(a), Δt decreased slightly with the increase of V_{inst}. The reduction of Δt was clearly observed at $V_a = 30$ kVrms in Figure 4(b).

3.2 dc CONDITION

Figure 5 shows the typical time-resolved PD characteristics under positive dc condition at (a) $V_a = 25$ kV, (b) $V_a = 30$ kV and (c) $V_a = 40$ kV. Note that the PD inception voltage under positive dc condition was 23 kV. As seen in Figure 5(a), the sequential generation of PD was observed, as it was in the case of ac in Figure 2(a). After the applied voltage was increased at $V_a = 30$ kV in Figure 5(b), only PD with relatively small magnitudes of charge occurred and the repetition rate of PD generation increased. The repetition rate of PD generation further increased at $V_a = 40$ kV in Figure 5(c).

Figure 6 shows the applied voltage dependence of the time interval Δt between subsequent PD pulses. Note that Δt is the reciprocal of the repetition rate, and that the vertical range lines show the min/max values of the obtained data. In Figure 6, Δt gradually decreased with the increase of the applied voltage, which also corresponds to the result under ac conditions in Figure 4(b).

4 DISCUSSION

4.1 CORONA STABILIZATION EFFECT UNDER ac CONDITION

As shown in Figure 3, the charge magnitude of the first PD was proportional to the instantaneous voltage V_{inst} and was independent of the applied ac voltage V_a. This is related to the size of the critical volume

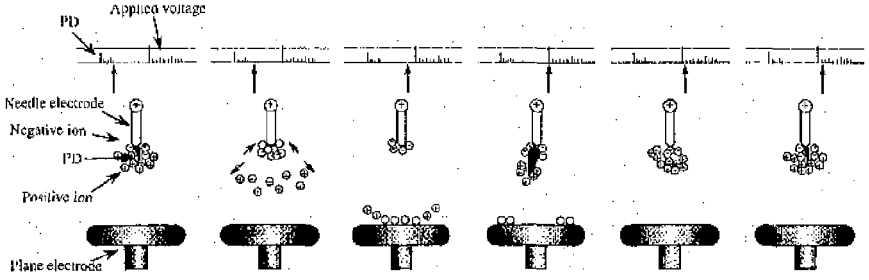

Figure 10. Schematic illustration of the generation mechanism of the first and subsequent PD under lower +dc condition.

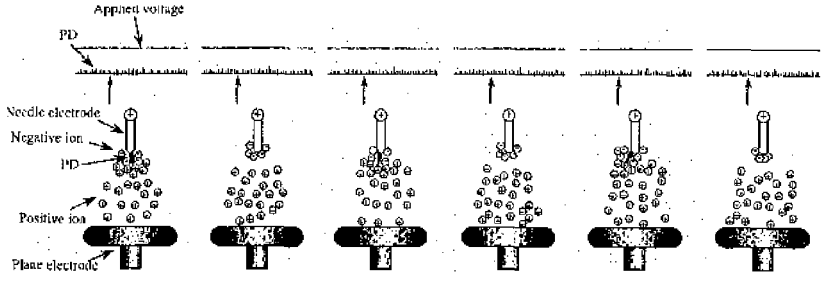

Figure 11. *Schematic illustration of the generation mechanism of the PD under higher +dc condition.*

and the statistical time lag. Note that the critical volume means the volume where the electric field strength is higher than the critical electric field of discharge inception in SF_6 gas (87.8 V/(Pa m).

The generation mechanism of the first and second PD is shown schematically in Figure 7. The ions generated by PD in the previous negative half cycle reached both electrode surfaces and most of them were neutralized at the polarity reversal of the applied ac voltage with the commercial power frequency [10]. The residual ions contribute to the generation of the positive PD in the subsequent positive half cycle. The charge magnitude of the first PD would be proportional to the size of the critical volume, namely the instantaneous voltage. The scattering of V_{inst} is related to the probability of the generation of an initial electron.

In contrast, PD subsequent to the first PD had small charges. This is due to the corona stabilization effect. The first PD generates many positive ions at the needle tip, which reduce the electric field strength at the needle tip. Therefore, the ionization by PD is restrained and only PD with small charges occur. Here, the increase of V_{inst} raises the probability of PD generation due to the enhancement of the electric field strength at the needle tip and the concentration of negative ions at the needle tip. Thus, the time interval Δt between sequential PD would be reduced in Figure 4.

4.2 CORONA STABILIZATION EFFECT UNDER dc CONDITION

4.2.1 LOWER VOLTAGE CONDITION

In this Section, we discuss the PD behavior under positive dc condition at $V_a = 25$ kV in Figure 5(a). In the Figure, we can clearly identify that there are two clusters of PD pulse generation. In each cluster, the first PD with large charge can be distinguished from the subsequent PD with small charge. Here, the time interval Δt_1 and Δt_2 are defined as shown in Figure 8; the first PD with the charge q_1 occurs at Δt_1 after the last PD in the previous PD cluster, while the second PD with q_2 occurs at Δt_2 after the first PD in the identical PD cluster.

Figure 9 shows the relationship between q_1 and Δt_1 (referred to as q_1 *vs.* Δt_1, hereinafter) and also q_2 and Δt_2 (q_2 *vs.* Δt_2) at $V_a = 25$ kV. As seen in Figure 9, the first PD and the second PD can be distinguished clearly by both the charge magnitude and the time interval between PD pulses. In Figure 9, q_1 depends on Δt_1. On the other hand, the second PD had smaller q_2 and shorter Δt_2 compared with those for the first PD. This difference depends on the contribution of the corona stabilization effect. The generation mechanism of the first and subsequent PD is schematically illustrated in Figure 10. As the time without PD generation goes on, the number of ions at the needle tip decreases due to the drift and diffusion of ions and then, the corona stabilization effect becomes weaker. Once an initial electron is created, PD with a large charge occurs, which newly generates a large number of positive and negative ions. Since the positive ions activate the corona stabilization, PD with the small charge follow the first PD. This mechanism is similar to that observed at positive PD inception phase under ac condition in Figure 7.

4.2.2 HIGHER VOLTAGE CONDITION

The sequential generation of the first and subsequent PD cannot be recognized under dc at $V_a = 30$ kV and $V_a = 40$ kV in Figure 5(b) and (c). In these conditions, PD with relatively small charge were observed. This is due to the highly activated corona stabilization effect. The PD generation mechanism observed at such higher voltage condition is shown schematically in Figure 11. A large number of positive ions as well as negative ions exist in the gap space. The positive ions reduce the electric field strength at the needle tip, resulting in the suppression of the ionization during the PD extension. On the contrary, a large amount of negative ions in the critical volume enlarges the creation probability of an initial electron due to the increase in the col-

lisional detachment probability. Moreover, the increase of the applied voltage enlarges the critical volume, *i.e.* the probability of the PD generation. Therefore, the time interval Δt between sequential PD decreases as in Figure 6.

5 CONCLUSIONS

In this paper, we measured the sequential generation of PD pulses in order to discuss the space charge behavior and the corona stabilization effect in SF_6 gas under ac and dc conditions. Consequently, we demonstrated the following.

1. The sequential generation of PD shows the larger magnitude of the first PD and the smaller magnitude of subsequent PD.
2. The charge of the first PD under ac condition depends on the instantaneous voltage.
3. Subsequent PD have small charges, independent of the instantaneous voltage.
4. The charge of the first PD under dc condition depends on the time interval between PD pulses.
5. Positive ions suppress the ionization during the PD extension and activate the corona stabilization effect.
6. Negative ions are a cause of an initial electron and decrease the time interval between PD pulses.

ACKNOWLEDGMENT

This research was supported in part by the Proposal-Based New Industry Creative Type Technology R&D Promotion Program from the New Energy and Industrial Technology Development Organization (NEDO) of Japan.

REFERENCES

[1] S. Yanabu, Y. Murayama and S. Matsumoto, "SF_6 Insulation and Its Application to HV Equipment", IEEE Trans. on Elect. Insul., Vol. 26, No. 3, pp. 358–366, 1991.

[2] M. Koto, S. Okabe, T. Kawashima, T. Yamagiwa and T. Ishikawa, "Insulation Characteristics of GIS for Non-Standard Lightning Surge Waveforms", Proc. 8th Int. Symp. on Gaseous Dielectrics VIII, pp. 547–553, 1998.

[3] R. Baumgärtner, B. Fruth, W. Lanz and K. Petterson, "Partial Discharge - Part IX: PD in Gas-Insulated Substation - Fundamental Considerations", IEEE Elect. Insul. Magazine, Vol. 7, No. 6, pp. 5–13, 1991.

[4] H. Okubo, T. Kato, N. Hayakawa and M. Hikita, "Temporal Development of Partial Discharge and Its Application to Breakdown Prediction in SF_6 Gas", IEEE Trans. on Power Deliv., Vol. 13, No. 2, pp. 440–445, 1998.

[5] T. Utsumi, F. Endo, T. Ishikawa, S. Iwaasa and T. Yamagiwa, "Preventive Maintenance System with a Different Gas Injecting Facility for GIS", IEEE Trans. on Power Deliv., Vol. 8, No. 3, pp. 1107–1113, 1993.

[6] H. Muto, M. Doi, H. Fujii and M. Kamei, "Frequency Spectrum Due to Standing Waves Excited by Partial Discharges in a GIS", Proc. 10th Int. Symp. on High Voltage Eng., Vol. 4, pp. 179–182, 1997.

[7] B. F. Hampton, J. S. Pearson, C. J. Jones and T. Irwin, "Experience and Progress with UHF Diagnostics in GIS", CIGRE 1992 Session 15/23–03, 1992.

[8] X. Han, Y. Wang, L. G. Chiristophorou and R. J. Van Brunt, "Characteristics of Partial Discharge on a Dielectric Surface in SF_6-N_2 Mixtures", Proc. 8th Int. Symp. on Gaseous Dielectrics VIII, pp. 307–312, 1998.

[9] H. Okubo, M. Yoshida, T. Takahashi, M. Hikita, H. Watanabe and N. Hashimoto, "Investigation of Partial Discharge Mechanism in SF_6 gas by Simultaneous Measurement of Current Waveform and Light Emission", Proc. 10th Int. Symp. on High Voltage Eng., Vol. 2, pp. 177–180, 1997.

[10] T. Takahashi, T. Yamada, M. Hikita and H. Okubo, "Dependence of Partial Discharge and Breakdown Characteristics on Applied Power Frequency in SF_6 Gas", Proc. 8th Int. Symp. on Gaseous Dielectrics VIII, pp. 295–300, 1998.

Manuscript was received on 13 November 1998, in revised form 21 December 1999.